High-efficiency DBA-BOTDA with optimized SNR by multiple bandwidths pump modulation

Huiliang Ma (马辉亮), Xinhong Jia (贾新鸿)*, Kai Lin (林 凯), and Cong Xu (徐 聪)

College of Physics and Electronic Engineering, Sichuan Normal University, Chengdu 610101, China
**Corresponding author: jiaxh_0@126.com*

Received September 18, 2018; accepted November 12, 2018; posted online December 20, 2018

For Brillouin optical time-domain analysis (BOTDA) based on distributed Brillouin amplification (DBA), constant Brillouin response achieved by the exponentially variable bandwidth/intensity pump modulation suffers from the much lower pumping efficiency for long-range sensing, which counterbalances the merit of DBA. In this Letter, pump modulation by multiple constant bandwidths was proposed and demonstrated. The ~98.9 km sensing with ~5 m spatial resolution and no use of optical pulse coding (OPC) was achieved by ~8 dBm Brillouin pump, which is lower by ~9 dB in theory by comparison with exponentially increased bandwidth modulation. Compared with traditional DBA-BOTDA, signal-to-noise ratio (SNR) enhancement with >4.6 dB was obtained. The flattened standard deviation (STD) of Brillouin frequency shift (BFS) (less than ~2 MHz) along the whole fiber was demonstrated.

OCIS codes: 060.4370, 290.5900.
doi: 10.3788/COL201917.010603.

Brillouin optical time-domain analysis (BOTDA) sensors based on stimulated Brillouin scattering (SBS) have been paid much attention in the past two decades, due to their ability to monitor temperature and strain distributions along the sensing fiber[1,2]. In practice, it can be applied in several fields, including structure health monitoring, fire alarming, oil pipeline leaking, power establishment security monitoring, etc.

For standard BOTDA, in order to compensate for the reduction of the signal-to-noise ratio (SNR) caused by intrinsic attenuation, the peak power of pulse and Stokes power injected into the fiber under test (FUT) must be higher. However, the practical pulse peak power is limited to ~20 dBm due to the pulse peak decrease caused by modulation instability (MI)[3] and spectral expansion caused by self-phase modulation (SPM)[4]. The Stokes power is also limited to ~−10 dBm in dual-sideband BOTDA, due to the high-order non-local effect[5].

Several first- or second-order pumping configurations based on distributed Raman amplification (DRA)[6–12] and distributed Brillouin amplification (DBA)[13–24] have been proposed for enhancing the SNR of distributed sensors. By comparison, DBA is more superior in terms of much higher pumping efficiency (pump power at the milliwatt level) and reduced pump-to-pulse relative intensity noise (RIN) transfer.

In traditional DBA-BOTDA, a widened bandwidth (a few hundreds of megahertz) based on uniform frequency modulation (FM)[14,16,18] or optical frequency comb (OFC)[13,15,17] was often utilized to avoid the pulse distortion. However, there exists a wide region with lower SNR due to the intrinsic loss, resulting in the larger standard deviation (STD) of Brillouin frequency shift (BFS) in this range[13–17].

Recently, a tailored pump compensation scheme was proposed in DBA-BOTDA sensors to achieve the flattened Brillouin response and SNR over FUT[18]. In this scheme, unlike uniform bandwidth modulation, a laser diode with exponentially increased bandwidth (through FM induced by current change) from 200 MHz to 2 GHz was used to control its spectral density, and thus the Brillouin gain coefficient was decreased exponentially along the fiber to compensate for the loss, making the Brillouin response approach a constant. A sensing distance of 51.2 km using ~11 dBm Brillouin pump has been realized[18]. A similar sensing distance of 50 km with flattened Brillouin response was reported by the authors using exponentially decreased intensity modulation (IM) for the pump (~8 dBm)[19].

However, for DBA-BOTDA with constant Brillouin response, further extension of sensing distance far beyond 50 km requires the significantly intensified pump power, as it is increased exponentially with the length of the FUT (see the analysis below). For example, 10 dB increments are required for 100 km sensing. This greatly counterbalances the high-efficiency advantage of DBA.

Moreover, for exponential bandwidth modulation, its dynamic range should also be increased to 20 dB (for example, from 100 MHz to 10 GHz). It is technically difficult to be realized due to the detrimental parasitical amplitude change of the laser diode[18]. Similarly, exponential IM of the Brillouin pump[19] up to 20 dB dynamic range is also challenged technically.

In this Letter, a new design of pump modulation by multiple constant bandwidths is proposed and presented. The simultaneously enhanced pumping efficiency by ~9 dB in theory (compared with the exponential bandwidth/IM) and enhanced SNR with >4.6 dB (compared with the standard DBA-BOTDA) are achieved.

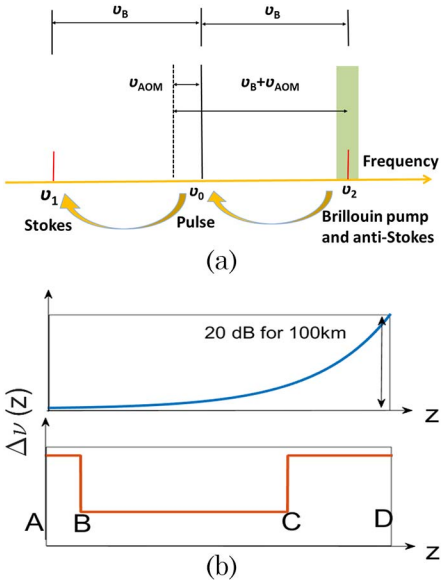

Fig. 1. (a) Schematic diagram of DBA-BOTDA with pump bandwidth modulation. (b) Pump bandwidth ($\Delta\nu$) distribution with exponential variation (blue) and proposed design with multiple bandwidths modulation (red). In (a), the position of the dotted line denotes the frequency of the optical source.

Figure 1(a) gives the schematic diagram of DBA-BOTDA with pump bandwidth modulation. The position of the dotted line denotes the frequency of the optical source. Due to the frequency shift (ν_{AOM}) of the acoustic-optic modulator (AOM), the frequency shift of the Brillouin pump (ν_2) relative to the optical source should be $\nu_B + \nu_{\mathrm{AOM}}$, where ν_B is equal to BFS. Since an acoustic-optic frequency shifter (AOFS) with the same frequency of ν_{AOM} is also introduced for the Stokes wave (ν_1), the frequency shift of the Stokes component relative to the optical source should be scanned around ν_B.

In Fig. 1(b), the pump bandwidth ($\Delta\nu$) distribution with exponential variation is described by the blue line, whereas the proposed modulation distribution by multiple constant bandwidths is denoted with the red line. Considering the higher pulse power in the front end (AB), it is not necessary to strongly amplify the pulse. In section BC, considering the larger loss for both the pulse and Brillouin pump, the modulation bandwidth should be lower to generate the larger gain coefficient. For the section of the far end (CD), the power of the Brillouin pump is higher, thus the wider bandwidth is expected in order to suppress the nonlinear effects induced by excessive pulse amplification.

Assuming that the pulse light and Brillouin pump are injected at $z = 0$ and $z = L$, respectively, the evolutions of pulse peak power (P_p) and Brillouin pump power (P_B) are governed by the following equations:

$$P_p(z) = P_p(0)\exp(-\alpha z)\exp\left[\int_0^z g_{\mathrm{BP}}(\xi)P_B(\xi)\mathrm{d}\xi\right], \quad (1)$$

$$P_B(z) = P_B(L)\exp[-\alpha(L-z)], \quad (2)$$

where L is the length of the FUT, and α is the loss coefficient. In Eqs. (1) and (2), due to the approximately symmetrical dual-sideband Stokes and anti-Stokes power distribution, the second-order non-local effect can be reasonably ignored. In addition, because of the limited pulse energy, the Brillouin pump depletion by a single pulse is also ignored[13]. The pump-to-pulse gain coefficient g_{BP} is determined by the distribution of the pump bandwidth[18,25],

$$g_{\mathrm{BP}}(z) = \frac{g_0}{1+\frac{\Delta\nu(z)}{\Delta\nu_B}} \to \frac{g_0}{\frac{\Delta\nu(z)}{\Delta\nu_B}} \qquad (\text{if } \Delta\nu \gg \Delta\nu_B), \quad (3)$$

where g_0 is the Brillouin gain coefficient with sufficiently smaller pump bandwidth, and $\Delta\nu_B$ is the intrinsic bandwidth of the Brillouin gain.

The constant Brillouin response can be achieved when $g_{\mathrm{BP}}(z) \times P_B(z) \equiv \alpha$. From Eqs. (2) and (3), the following condition should be satisfied[18]:

$$\Delta\nu(z) = \Delta\nu(0)\exp(\alpha z), \quad (4a)$$

$$P_B(L) = \frac{\alpha\Delta\nu(0)}{g_0\Delta\nu_B}\exp(\alpha L). \quad (4b)$$

For exponentially decreased IM for constant Brillouin response, a same formula with Eq. (4b) can be derived.

For our proposed multiple constant bandwidths, at transparency transmission, i.e., $P_p(L) = P_p(0)$, we have

$$P_B(L) = \frac{\alpha L}{g_0\Delta\nu_B\left\{\frac{L_{\mathrm{eff}}^{\mathrm{AB}}\exp[-\alpha(L_{\mathrm{BC}}+L_{\mathrm{CD}})]}{\Delta\nu_{\mathrm{AB}}} + \frac{L_{\mathrm{eff}}^{\mathrm{BC}}\exp[-\alpha L_{\mathrm{CD}}]}{\Delta\nu_{\mathrm{BC}}} + \frac{L_{\mathrm{eff}}^{\mathrm{CD}}}{\Delta\nu_{\mathrm{CD}}}\right\}}, \quad (5a)$$

where L_i and $\Delta\nu_i$ are the length and pump bandwidth of each subsection. L_{eff}^i is the effective length given by

$$L_{\mathrm{eff}}^i = \frac{1-\exp(-\alpha L_i)}{\alpha} \qquad (i = \mathrm{AB}, \mathrm{BC}, \mathrm{CD}). \quad (5b)$$

By comparison of Eqs. (4b) and (5a), it is clear that the exponential pump power requirement with the increased L in the case of constant Brillouin response is now replaced by the non-exponential relationship in the proposed design.

The measured (squared) and fitted (solid) pump-to-pulse gain coefficient as a function of pump bandwidth is shown in Fig. 2. During the curve fitting with Eq. (3), $\Delta\nu_B = 30$ MHz. Using the extracted $g_0 = 0.337\ \mathrm{m}^{-1}\cdot\mathrm{W}^{-1}$, for constant Brillouin response along the 100 km fiber, the required pump power is estimated to be 17 dBm when $\Delta\nu(0) = 120$ MHz. In contrast, for our proposed design, when $L_{\mathrm{AB}} = 10$ km, $L_{\mathrm{BC}} = 60$ km, $L_{\mathrm{CD}} = 30$ km, $\Delta\nu_{\mathrm{AB}} = \Delta\nu_{\mathrm{CD}} = 320$ MHz, and $\Delta\nu_{\mathrm{BC}} = 120$ MHz, the required pump power is 7.9 dBm. These data are close to the optimized conditions in the experiment. Hence, the enhanced pumping

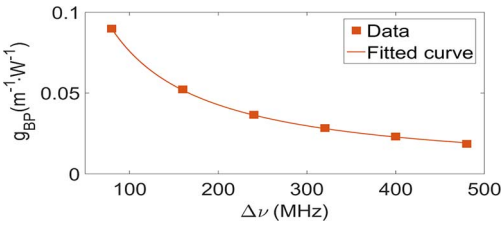

Fig. 2. Measured (squared) and fitted (solid) pump-to-pulse gain coefficient as a function of pump bandwidth.

efficiency by ~9 dB in theory can be achieved by the proposed design.

The experimental setup of DBA-BOTDA using pump modulation is depicted in Fig. 3. A 1549.2 nm distributed feedback laser diode (DFB-LD) is used as an optical source. The Brillouin pump is generated by an electro-optic modulator 1 (EOM1) driven by an FM microwave source (MWS). Here, FM modulation is realized by an in-phase quadrature (IQ) modulator module, represented in a green square in this diagram. The generated microwave signal $V_{\mathrm{FM}}(t)$ takes the form of

$$\begin{aligned} V_{\mathrm{FM}}(t) &= V_0\cos[(2\pi\nu_{\mathrm{MSW1}}t)+\varphi(t)] \\ &= V_0\{\cos(2\pi\nu_{\mathrm{MSW1}}t)\cos[\varphi(t)] \\ &\quad -\sin(2\pi\nu_{\mathrm{MSW1}}t)\sin[\varphi(t)]\}, \end{aligned} \tag{6a}$$

where V_0 is the amplitude, $\nu_{\mathrm{MSW1}}=\nu_B+\nu_{\mathrm{AOM}}$ is the frequency of MWS1. The modulation phase $\varphi(t)$ is determined by the instantaneous frequency offset of FM, $\delta\nu(t)$, expressed by

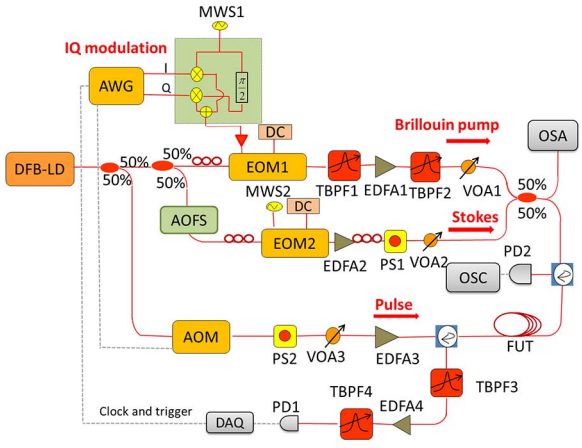

Fig. 3. Experimental setup of DBA-BOTDA using pump modulation. DFB-LD, distributed feedback laser diode; EOM, electro-optic modulator; EDFA, erbium-doped fiber amplifier; PS, polarization scrambler; VOA, variable optical attenuator; FUT, fiber under test; AOM, acoustic-optic modulator; AOFS, acoustic-optic frequency shifter; AWG, arbitrary waveform generator; MWS, microwave source; TBPF, tunable bandpass filter; PD, photodetector; DAQ, data acquisition; OSA, optical spectrum analyzer; OSC, oscilloscope.

$$\varphi(t)=\varphi_0+2\pi\int_0^t\delta\nu(\tau)\mathrm{d}\tau, \tag{6b}$$

where φ_0 is the initial phase. Since EOM1 operates at a carrier suppressed point, the low-frequency sideband is removed by a tunable bandpass filter 1 (TBPF1). In the experimental setup, ν_B and ν_{AOM} are ~10, 845 and 200 MHz, respectively, so ν_{MSW1} is fixed at 11,045 MHz.

The optical pulse with ~50 ns width is formed by an AOM, driven by the output of the arbitrary waveform generator (AWG). The extinction ratio and rising time of the AOM are 52 dB and 8 ns, respectively. The Stokes and anti-Stokes components are generated by EOM2, which operates at a carrier suppressed point. As mentioned above, an AOFS is introduced to compensate for the frequency shift of the AOM, so the scanning frequency of MWS2 is around ν_B. Three erbium-doped fiber amplifiers (EDFAs) are used to boost the injected optical powers. To cancel out the impact of noise from polarization dependent gain, two polarization scramblers (PS1 and PS2) are used in Stokes and pulse branches.

In Fig. 3, the transmitted Brillouin pump, anti-Stokes component, and Rayleigh scattering of pulse light are eliminated by TBPF3. EDFA4 acts as the pre-amplifier of Stokes light. The amplified spontaneous emission (ASE) is then filtered out by TBPF4. The bandwidth of photodetector 1 (PD1) and the sampling rate of the data acquisition card are 100 MHz and 100 MSa/s, respectively. The real-time waveform of the transmitted pulse is detected and monitored by wideband PD2 and an oscilloscope.

Figure 4 displays the instantaneous frequency offset of FM applied to generate multiple bandwidths pump modulation. The fiber is divided into three parts with the duration times of 100, 600, and 300 μs, corresponding to the length of 10, 60, and 30 km, respectively. The period of the produced saw-tooth FM waveform is 1 μs, as shown in the inset of Fig. 4. Note that the pulse has 500 μs delay (flight time of pump) to undergo the initial amplification. Often, the variation region of BFS within section BC is typically smaller than hundreds of meters; thus, the pulse gain variation in these regions is also small.

Figures 5(a) and 5(b) report the measured Brillouin gain spectra (BGSs) for conventional and proposed DBA-BOTDAs, respectively. During measurement, the Stokes and pulse peak powers are set to ~−10 and 20 dBm, respectively. The frequency scanning range of

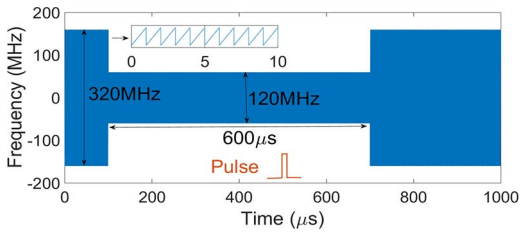

Fig. 4. Instantaneous frequency offset of FM applied to generate the multiple bandwidths pump modulation.

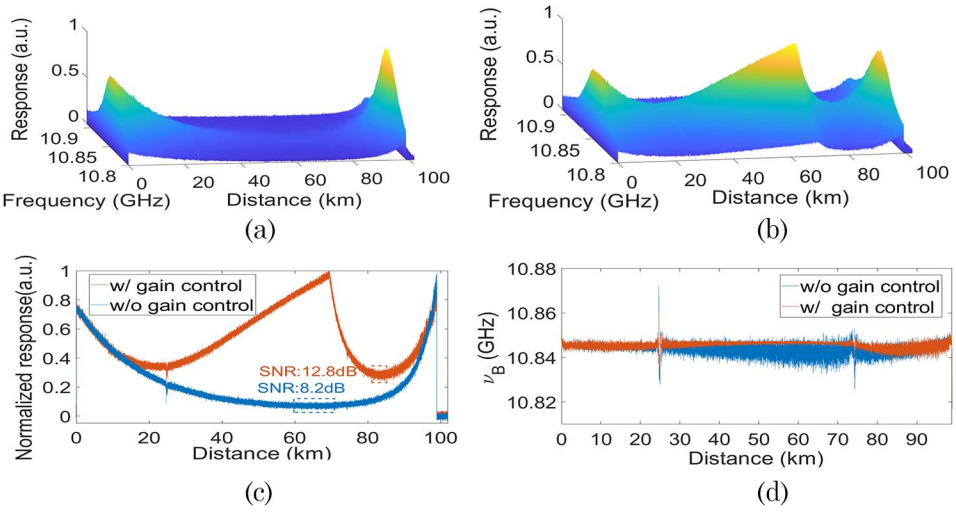

Fig. 5. (a) BGS of conventional DBA-BOTDA. (b) BGS of proposed DBA-BOTDA. (c) Comparison of Brillouin responses at 10,845 MHz. (d) Comparison of extracted BFS distributions. In (c) and (d), blue and red lines correspond to pump modulation with constant bandwidth and multiple bandwidths, respectively.

MWS2 is 10,800–10,910 MHz with 5 MHz steps. Trace average by 12,000 times is carried out to reduce the noise. For conventional DBA, the constant pump bandwidth is 120 MHz. The required pump powers for transparency transmission of the pulse are ~5 and ~8 dBm, respectively, in Figs. 5(a) and 5(b), which are in good agreement with theoretical predictions. A wide and deep valley over the range of 40–80 km occurs in the conventional DBA-BOTDA. After using multiple constant bandwidths modulation, the depths of two valleys are strongly diminished.

The trace comparison at 10,845 MHz is presented in Fig. 5(c). In the range with minimal Brillouin response, the SNRs of conventional and proposed DBA-BOTDA are ~8.2 and ~12.8 dB, respectively. Thus, the least SNR enhancement of ~4.6 dB is achieved. Here, the SNR is calculated based on the ratio of the signal and the STD of noise[26]. Note that the range with lower SNR is also narrowed sharply across the FUT. The extracted BFS distributions after Lorentz fitting are shown in Fig. 5(d). It is found that the larger BFS fluctuation caused by the worsened SNR in the range of 40–80 km is eliminated by the proposed design.

By performing the repeated measurement eight times, the STD of BFS is calculated and shown in Fig. 6. The maximal STDs of conventional and proposed DBA-BOTDAs are close to ~4 and ~2 MHz, respectively. Particularly, the STD across the range of 0–70 km is less than ~1 MHz for the proposed design. The slightly increased STD for the last 10 km is caused by the expanded bandwidth (~70 MHz maximum) due to SPM.

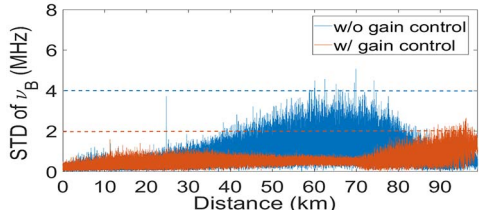

Fig. 6. STD of BFS for conventional DBA-BOTDA (blue) and multiple bandwidths pump modulation (red).

Figures 7(a) and 7(b) show the recorded pulse waveforms after FUT without (red) and with (blue) DBA for different pulse peak powers. The delay due to slow light is ~5 ns, corresponding to ~0.5 m spatial resolution degradation. For the case of 14 dBm pulse peak power [see Fig. 7(b)], pulse distortion due to DBA is slight. A smaller distortion of slowed rising time is observed for the pulse peak power of 20 dBm [see Fig. 7(a)]. This observation results from the phonon response time (~10 ns) during amplification.

We note that the impact of pulse distortion on sensing performance is also smaller, as proved in Figs. 7(c) and 7(d), where the BFS distributions for various pulse peak powers are shown. When the pulse peak is increased from 14 to 20 dBm, except for decreased BFS fluctuation, their distributions are almost overlapped for 0–94 km; the BFS deviation for 20 dBm pulse peak is less than ~1.5 MHz for the last 5 km (relative to that at 14 and 17 dBm). This smaller deviation is caused by the pulse frequency shift due to SPM of the distorted pulse[14,16]. Similar waveform change can be found in Figs. 8(a) and 8(b) for traditional constant bandwidth pumping.

We then introduced a hot spot 5 m long at the end of the FUT. The room temperature is kept at ~25.8°C. The hot spot is heated in a water-bath thermostat with the 10°C step. The pulse peak power is 20 dBm according to the analysis in Fig. 7. Figure 9(a) shows the BFS of the hot spot as a function of temperature. A good linear relationship is obtained. The measured sensitivity by linear fitting is ~1.064 MHz/°C. The extracted temperature distribution around the hot spot (~55.8°C) is shown in Fig. 9(b).

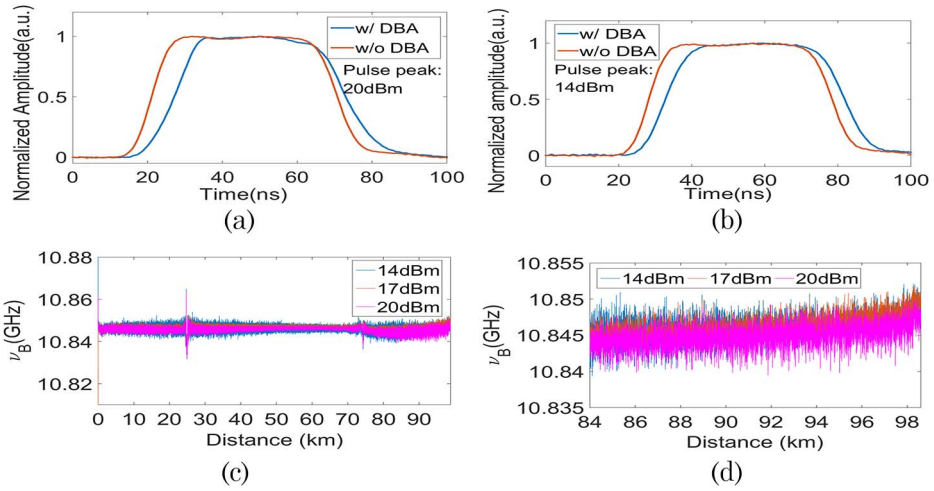

Fig. 7. (a), (b) Recorded pulse waveforms after transmission without (red) and with (blue) DBA for different pulse peak powers. (c) BFS distributions for various pulse peak powers. (d) The detail of BFS for the far end. Measurement is executed for the proposed multiple bandwidths pulse modulation.

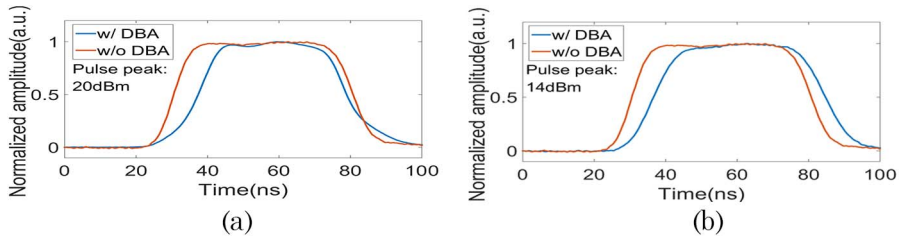

Fig. 8. Recorded pulse waveforms after transmission without (red) and with (blue) DBA for different pulse peak powers. Conventional constant bandwidth pumping is used.

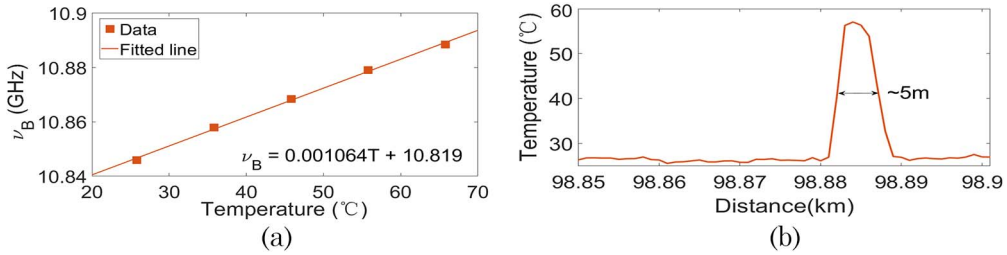

Fig. 9. (a) BFS of the hot spot as a function of temperature. (b) Extracted temperature distribution around the hot spot (~55.8°C). Multiple bandwidths modulation is used.

The ~5 m spatial resolution is confirmed by the full width at half-maximum (FWHM) of the hot spot.

Figure 10 shows the Brillouin traces for different lengths of L_{AB} and L_{CD}. The larger gain fluctuations are found when L_{AB} is 20 km and L_{CD} is ~20 km, or L_{AB} is 30 km and L_{CD} is ~10 km due to larger loss in section AB.

In conclusion, a pump modulation design using multiple constant bandwidths was proposed and demonstrated for extending the sensing range of DBA-BOTDA without sacrificing the pumping efficiency. Compared with the exponential bandwidth/IM, pumping efficiency improvement of ~9 dB can be obtained. Also, this design can avoid the requirement of a larger bandwidth range. Meanwhile, compared with conventional DBA-BOTDA, SNR

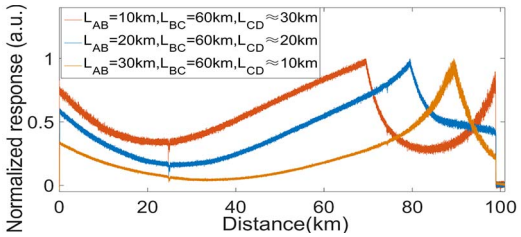

Fig. 10. Brillouin traces for different combinations of L_{AB} and L_{CD}.

enhancement with >4.6 dB along ~98.9 km sensing fiber has been confirmed by the experiment. The spatial resolution of ~5 m and flattened STD distribution of

Table 1. FOM of Refs. [13–18] and This Work

Refs.	[13][a]	[14][b]	[15][c]	[16][d]	[17][e]	[18][f]	This work
FOM	2108	6	6	1240	235	40	151

[a] L: 123.6 km; Δz: 5 m; σ_ν: 1.6 MHz; N_{av}: 6700; δ: 5 MHz; $\Delta\nu_B$: 50 MHz.
[b] L: 50 km; Δz: 1.5 m; σ_ν: 0.6 MHz; N_{av}: 4096; δ: 1 MHz; $\Delta\nu_B$: 32 MHz.
[c] L: 49.5 km; Δz: 3.2 m; σ_ν: 1.6 MHz; N_{av}: 1200; δ: 3 MHz; $\Delta\nu_B$: 75 MHz.
[d] L: 100 km; Δz: 1 m; σ_ν: 1 MHz; N_{av}: 1500; δ: 1.6 MHz; $\Delta\nu_B$: 30 MHz.
[e] L: 99 km; Δz: 5 m; σ_ν: 1.6 MHz; N_{av}: 4500; δ: 4 MHz; $\Delta\nu_B$: 50 MHz.
[f] L: 51.2 km; Δz: 20 cm; σ_ν: 1.45 MHz; N_{av}: 4096; δ: 2 MHz.

BFS (less than ∼2 MHz) have been achieved without the use of optical pulse coding (OPC). Using Eq. (10) of Ref. [27], a list of the figure of merit (FOM) for Refs. [13–18] and this work is shown in Table 1, where Δz is the spatial resolution, σ_ν is the STD of BFS, N_{av} is the average time, δ is the scanning step, and $\Delta\nu_B$ is the FWHM of BGS. We believe if OPC is combined to further enhance the SNR, sensing distance extension far beyond 100 km could be expected.

This work was supported by the National Natural Science Foundation of China (NSFC) (No. 61205079) and the Scientific Research Fund of Sichuan Provincial Education Department (No. 18ZA0401). The authors thank Dr. Javier Urricelqui, Dr. Juan José Mompó, and Prof. Alayn Loayssa at the Universidad Pública de Navarra for providing the data from Refs. [14,16].

References

1. M. J. Zhang, X. Y. Bao, J. Chai, Y. N. Zhang, R. X. Liu, H. Liu, Y. Liu, and J. Z. Zhang, Chin. Opt. Lett. **15**, 080603 (2017).
2. B. Wang, X. Y. Fan, J. B. Du, and Z. Y. He, Chin. Opt. Lett. **15**, 120601 (2017).
3. M. Alem, M. A. Soto, and L. Thévenaz, Opt. Express **23**, 29514 (2015).
4. S. M. Foaleng, F. Rodríguez-Barrios, S. Martin-Lopez, M. González-Herráez, and L. Thévenaz, Opt. Lett. **36**, 97 (2011).
5. J. Urricelqui, M. Sagues, and A. Loayssa, Opt. Express **21**, 17186 (2013).
6. X. H. Jia, Y. J. Rao, L. Chang, C. Zhang, and Z. L. Ran, J. Lightwave Technol. **28**, 1624 (2010).
7. F. Rodríguez-Barrios, S. Martín-López, A. Carrasco-Sanz, P. Corredera, J. D. Ania-Castañón, L. Thévenaz, and M. González-Herráez, J. Lightwave Technol. **28**, 2162 (2010).
8. X. H. Jia, Y. J. Rao, K. Deng, Z. X. Yang, L. Chang, C. Zhang, and Z. L. Ran, IEEE Photon. Technol. Lett. **23**, 435 (2011).
9. S. Martin-Lopez, M. Alcon-Camas, F. Rodriguez, P. Corredera, J. D. Ania-Castañon, L. Thévenaz, and M. Gonzalez-Herraez, Opt. Express **18**, 18769 (2010).
10. X. H. Jia, Y. J. Rao, Z. N. Wang, W. L. Zhang, C. X. Yuan, X. D. Yan, J. Li, H. Wu, Y. Y. Zhu, and F. Peng, Opt. Express **21**, 21208 (2013).
11. X. H. Jia, Y. J. Rao, C. X. Yuan, J. Li, X. D. Yan, Z. N. Wang, W. L. Zhang, H. Wu, Y. Y. Zhu, and F. Peng, Opt. Express **21**, 24611 (2013).
12. M. A. Soto, X. Angulo-Vinuesa, S. Martin-Lopez, S. H. Chin, J. D. Ania-Castañon, P. Corredera, E. Rochat, M. Gonzalez-Herraez, and L. Thévenaz, J. Lightwave Technol. **32**, 152 (2014).
13. K. Lin, X. H. Jia, H. L. Ma, C. Xu, X. Zhang, and L. Ao, Chin. Opt. Lett. **16**, 090604 (2018).
14. J. Urricelqui, M. Sagues, and A. Loayssa, Opt. Express **23**, 30448 (2015).
15. H. Q. Chang, X. H. Jia, X. L. Ji, C. Xu, L. Ao, H. Wu, Z. N. Wang, and W. L. Zhang, IEEE Photon. Technol. Lett. **28**, 1142 (2016).
16. J. J. Mompó, J. Urricelqui, and A. Loayssa, Opt. Express **24**, 12672 (2016).
17. X. H. Jia, H. Q. Chang, L. Ao, X. L. Ji, C. Xu, and W. L. Zhang, Opt. Express **24**, 14079 (2016).
18. Y. H. Kim and K. Y. Song, Opt. Express **25**, 14098 (2017).
19. X. H. Jia, K. Lin, and L. Ao, in *Asia Communications and Photonics Conference* (Optical Society of America, 2017), paper M3A.2.
20. E. Liokumovitch, D. Gotliv, and S. Sternklar, Opt. Lett. **42**, 5166 (2017).
21. D. Mermelstein, E. Shacham, M. Biton, and S. Sternklar, Opt. Lett. **40**, 3340 (2015).
22. H. J. He, B. Luo, X. H. Zou, W. Pan, and L. S. Yan, Opt. Express **26**, 23714 (2018).
23. Z. N. Wang, J. J. Zeng, J. Li, M. Q. Fan, H. Wu, F. Peng, L. Zhang, Y. Zhou, and Y. J. Rao, Opt. Lett. **39**, 5866 (2014).
24. Z. N. Wang, J. Li, M. Q. Fan, L. Zhang, F. Peng, H. Wu, J. J. Zeng, Y. Zhou, and Y. J. Rao, Opt. Lett. **39**, 4313 (2014).
25. G. P. Agrawal, *Nonlinear Fiber Optics* (Academic, 2007).
26. M. A. Soto, J. A. Ramírez, and L. Thévenaz, Nat. Commun. **7**, 10870 (2016).
27. M. A. Soto and L. Thévenaz, Opt. Express **21**, 31347 (2013).